

**THE ROLE OF PARTICLES IN THE INHIBITION OF PREMIXED FLAMES  
BY IRON PENTACARBONYL \***

Marc D. Rumminger<sup>†</sup>, Gregory T. Linteris<sup>‡</sup>

Building and Fire Research Laboratory

National Institute of Standards and Technology, Gaithersburg MD 20899, USA

Appears in *Combustion and Flame*, **123**(1/2):82-94, 2000.

**Running title: Role of Particles in Flame Inhibition by Iron**

**Corresponding author:**

Gregory T. Linteris  
National Institute of Standards and Technology  
Building and Fire Research Laboratory  
100 Bureau Dr.; Stop 8651  
Gaithersburg MD 20899-8651, USA

linteris@nist.gov  
ph: 301-975-2283  
fax: 301-975-4052

---

\* Official contribution of the National Institute of Standards and Technology, not subject to copyright in the United States.

<sup>†</sup> National Research Council/NIST postdoctoral fellow 1996-1998. Current address: Ceryx, Inc.; 1343 Main St.; Santa Paula, CA 93060;

<sup>‡</sup> Corresponding author.

## ABSTRACT

Laser light scattering has been used to investigate particle formation in  $\text{Fe}(\text{CO})_5$ -inhibited premixed flames in order to understand the influence of metal and metal oxide condensation on flame inhibition. In premixed  $\text{CH}_4$ -air flames, particles form early in the flame zone, nucleate and grow to a peak scattering cross section, then disappear as the temperature increases to its peak value. Downstream in the post-combustion gases, the peak scattering signal is several orders of magnitude larger than the peak value near the main reaction zone of the flame. Thermophoretic particle sampling and numerical estimates indicate nanoparticles with diameters between 10 and 30 nm. As the mole fraction of iron pentacarbonyl in the flame is increased, a concentration is reached at which both the burning velocity becomes constant and particle nucleation begins. A model of an ideal heterogeneous inhibitor shows that radical recombination on particle surfaces alone cannot account for the magnitude of the observed inhibition. Measurements in three  $\text{CO-H}_2$  flames with similar adiabatic flame temperatures but different burning velocities demonstrate the importance of residence time for particle formation in premixed flames.

## INTRODUCTION

The ban on production of the popular fire suppressants  $\text{CF}_3\text{Br}$  (halon 1301) and  $\text{CF}_2\text{ClBr}$  (halon 1211) and concerns about the effectiveness of short-term alternatives has led to renewed interest in understanding the mechanisms of non-fluorocarbon based, extraordinarily effective flame inhibitors, such as  $\text{Fe}(\text{CO})_5$  and dimethyl methylphosphonate (DMMP). Many of these compounds produce in-flame species with low vapor pressures, raising the likelihood of particle formation in the flame zone and therefore the possibility of heterogeneous chemistry. For  $\text{Fe}(\text{CO})_5$ , there have been conflicting claims in the literature as to whether the inhibition involves a gas-phase or heterogeneous mechanism [1-5]. Recent experimental [6] and numerical [5,7] results strongly suggest that the effect at low agent loading is from gas-phase chemistry, and that particle formation hinders inhibition processes. If it is found, however, that particulates contribute to the inhibition, then the search for halon alternatives could be directed toward chemicals that produce similar condensed-phase compounds.

Recent experiments with premixed and diffusion flames [6,8,9] have shown that  $\text{Fe}(\text{CO})_5$  has a strong inhibitory effect under certain conditions, but almost no effect under others. A critical part of the research on  $\text{Fe}(\text{CO})_5$  is to determine the optimal conditions for inhibition in order to avoid those in which the inhibitor loses its effectiveness. In premixed flames the inhibition varies with the  $\text{Fe}(\text{CO})_5$  concentration: at low concentration the burning velocity is strongly dependent on inhibitor mole fraction, whereas at high concentration the burning velocity is relatively independent

of inhibitor mole fraction. Additionally, numerical calculations using a gas-phase inhibition mechanism predict the behavior at low mole fraction reasonably well, but overpredict the inhibition at high mole fraction [5,10,11]. A plausible but unconfirmed explanation for this reduced effectiveness is that particles form and lower the gas-phase mole fraction of active inhibiting species [6].

Iron particle formation at high temperature has been studied for a variety of reasons. Iron pentacarbonyl is a popular precursor for shock tube studies of homogenous nucleation of iron and for the subsequent development of nucleation models [12-21]. The effect of iron additives on soot formation has been studied in laboratory scale diffusion flames [22-28], laboratory scale premixed flames [29-32], industrial furnaces [33], shock tubes [34,35] and internal combustion engines [23].  $\text{Fe}(\text{CO})_5$  has also been used as a precursor to manufacture particles and films [36-43]. Despite the breadth of research on iron particle formation, no one has investigated the effect of particles on flame inhibition by iron compounds.

In this paper we investigate iron condensation in non-sooting premixed flames. The regime is between the nearly reaction-free environment of the homogenous nucleation studies and the complex reaction zone of sooting flames. The primary motivation is to determine the effect of particle formation on flame inhibition. We use laser-light scattering to determine the particle formation region and to estimate the particle size. Thermophoretic sampling with transmission electron microscopy provide the particle size and morphology. The experiments use premixed Bunsen-type flames of  $\text{CH}_4\text{-O}_2\text{-N}_2$  and  $\text{CO-H}_2\text{-O}_2\text{-N}_2$ . By making proper choices of concentrations and gas

flows, the effects of both flame temperatures and residence time on particle formation are studied. The unresolved issue of whether the inhibition is heterogeneous or homogeneous is also addressed, and a model of an ideal heterogeneous inhibitor is presented.

## EXPERIMENTAL

### *Burner Systems*

The premixed burner system has been described previously [6,44]. Premixed flames ( $\phi=1.0$ ) are stabilized on a Mache-Hebra nozzle burner (inner diameter  $1.02 \text{ cm} \pm 0.005 \text{ cm}$ ) [45] with an air shroud flow. For the conditions investigated in this paper, the burner produces a steady, conical, non-sooting flame with a height of 13 mm. Measurements are made along a horizontal profile 7 mm above the burner base, which provides a pass through each side of the conical flame. The burner and shroud are housed in an acrylic chimney with three optical access holes. Rubber bellows connect the chimney with the adjacent optical elements to provide a flexible and airtight seal. The total gas flows to the burner are between 3.5 and 7.0 L/min for the uninhibited flames, and correspond to the conditions of the  $\text{Fe}(\text{CO})_5$  inhibition measurements described in Refs. [6] and [8].

Gas flows are measured with digital mass flow controllers (Sierra Model 860<sup>§</sup>) with a claimed repeatability of 0.2% and accuracy of 1% of full-scale flow, which have been calibrated with bubble (Gillian Gilibrator) and dry (American Meter Co. DTM-200A) flow meters so that their accuracy is 1% of indicated flow. The fuel gases are methane (Matheson UHP, 99.9% CH<sub>4</sub>), carbon monoxide (Matheson UHP, 99.9% CO, with the sum of CH<sub>4</sub> and H<sub>2</sub>O < 10 ppm<sup>\*\*</sup>) and hydrogen (Matheson UHP, 99.999% H<sub>2</sub>, with sum of N<sub>2</sub>, O<sub>2</sub>, CO<sub>2</sub>, CO, Ar, CH<sub>4</sub>, and H<sub>2</sub>O < 10 ppm). The oxidizer consists of nitrogen (boil-off from liquid N<sub>2</sub>) and oxygen (MG Industries, H<sub>2</sub>O < 50 ppm, total hydrocarbons < 5 ppm). All experiments are performed at ambient pressure and with gases at ambient temperature. Inhibitor is added to the flames by diverting part of the nitrogen (or methane) stream to a two-stage saturator maintained in an ice bath. The diverted gas (less than 8% of the total flow) bubbles through liquid Fe(CO)<sub>5</sub> and is saturated with Fe(CO)<sub>5</sub> vapor, before returning to the main nitrogen flow. The saturation mole fraction is determined from a correlation of Gilbert and Sulzmann [46], and the carrier gas was shown to be saturated with Fe(CO)<sub>5</sub> in previous work [8].

### *Optical System*

Light-scattering and extinction techniques with phase-sensitive detection are used to determine particle location and properties. The apparatus, shown in Figure 1, is similar

---

<sup>§</sup> Certain commercial equipment, instruments, or materials are identified in this paper to adequately specify the procedure. Such identification does not imply recommendation or endorsement by the National Institute of Standards and Technology, nor does it imply that the materials or equipment are necessarily the best available for the intended use.

<sup>\*\*</sup> All uses of ppm in this paper are on a volume basis and correspond to μmol/mol.

to those used by other researchers [47,48]. The light source is a 4-W argon-ion laser (Spectra Physics BeamLok 2060), with a vertically-polarized 2.2-W beam at 488 nm. A mechanical chopper (Stanford Research 640) modulates the beam at 1500 Hz and provides a reference signal for the lock-in amplifiers. A polarization-preserving single-mode optical fiber (3  $\mu\text{m}$  diameter) carries the light into a chemical fume hood (90 cm x 150 cm x 150 cm) which contains the burner. At the fiber output, collimating optics, a polarization rotator, mirrors and a focusing lens ( $f = 250$  mm) deliver the laser light to the test region. A glass wedge between the polarization rotator and the focusing lens diverts a small fraction of the beam to a reference detector which monitors the laser power during the experiments. The transmission efficiency for the laser-to-fiber coupling system is only about 15%, but this provides sufficient power for the experiments. The steep temperature gradients in the present flames cause significant beam steering and distortion. These effects, if unmitigated, would produce fluctuations of a few percent in the measured transmissivity, which is approximately the same magnitude as the peak absorptivity ( $< 2\%$ ). To reduce the beam steering effect, we follow an approach used by Dibble [49] and Nguyen [50], which involves reflecting the beam back through the flame along the same path, thus “unsteering” it. The approach has the additional benefit of doubling the path length and nearly doubling the laser light intensity at the focus. A concave spherical mirror ( $f = 250$  mm) reflects the beam back through the optical path and a glass wedge sends it to an integrating sphere. To spatially probe the flame, a three-axis translation stage (minimum step size of 0.0016 mm) positions the burner and chimney in the stationary optical path.

The light detection system consists of three photomultiplier tubes (PMT, all type 1P28) with appropriate filtering. The reference PMT has neutral density filters ( $OD \approx 6$ ) and a laser-line filter ( $\Delta\lambda = 10 \pm 2$  nm), and is typically operated at a voltage of  $-500$  V. The detection system for light scattered normal to the laser beam consists of a circular aperture (5 mm diameter), collection lens ( $f = 100$  mm), pinhole aperture (diameter 1 mm), laser-line filter, polarizer and PMT at  $-900$  V to  $-1000$  V. For the  $90^\circ$ -scattered light, the circular aperture (5 mm diameter) located 10 cm from the laser beam focus provides a solid angle of 0.002 sr. The pinhole aperture (1 mm diameter) defines the length of the sample to be 1 mm based on unity magnification.

The signal from each of the detectors is pre-amplified (Stanford Research 552) before entering a lock-in amplifier (Stanford Research 530). A personal computer controls the amplifiers and records the measurements during the experiments using a data acquisition card (Strawberry Tree DynaRes Ultra 8). In the data acquisition software, each scattering or transmission data point is normalized by the reference signal. Typically, 100 readings are averaged over a time of about 1 second; post-processing software reduces the data and calculates uncertainty as described below.

The measured quantities in the experiment are the voltage outputs of the reference, transmission, and scattered light detectors, and these depend on the system geometry, optical efficiencies, detector responsivity, gas density and particle number density, and the scattering cross section of the gases or particles. To obtain the scattering cross section ( $Q_{vv}$ ) of the gases or particles in the flame, a calibration of the optical system efficiency is performed using a gas with known scattering cross section

[47,48] (ethane is used because of its relatively large cross section,  $51.6 \times 10^{-28} \text{ cm}^2$  [51]).

The scattering and transmission signals are measured for the calibration gas to give a

calibration factor,  $C = Q_{vv,cal} \frac{\tau_{cal}}{S_{vv,cal}}$ , where  $Q_{vv,cal}$  is the known scattering cross section of

the calibration gas,

$\tau_{cal}$  is the transmissivity of the calibration gas, and  $S_{vv,cal}$  is the scattering signal caused by the calibration gas. Given the calibration constant and scattering

measurements, the scattering cross section at each location can be found as  $Q_{vv} = C \frac{S_{vv}}{\tau_{\lambda}}$ ,

where  $S_{vv}$  is the measured scattering signal and  $\tau_{\lambda}$  is the transmissivity of the flame gases and particles.

### *Thermophoretic Sampling*

Thermophoretic sampling with electron microscopy is used as a supplemental technique to determine particle size and morphology. The procedure and apparatus are similar to those used by Dobbins and Megaridis [52] and Koylu et al. [53], so limited details will be given here. A computer-controlled, double-acting piston with travel of 5.08 cm is used to quickly insert and remove the electron microscope (EM) grid from the flame. Transit times and the dwell time in the flame are measured using a laser, mirror, photodiode, and oscilloscope [53]. Each grid is attached to a stainless steel substrate with thickness of 0.4 mm, and height between 3 mm to 5.7 mm. The EM grids are

copper with a carbon film deposited on one side (Electron Microscopy Sciences p/n CFH4-SPEC-CU), and are fastened onto the metal substrates using adhesive or double-sided tape.

### ***Uncertainty Analysis***

The uncertainty analysis consists of calculation of individual uncertainty components and their root mean square sums [54], as outlined in Ref. [9]. All uncertainties are reported as *expanded uncertainties*:  $X \pm U$ , where  $U$  is  $ku_c$ , and is determined from a combined standard uncertainty (estimated standard deviation)  $u_c$ , and a coverage factor  $k = 2$  (level of confidence approximately 95%). Likewise, when reported, the relative uncertainty is  $U / X \cdot 100\%$ , or

$$ku_c / X \cdot 100\%.$$

The expanded relative uncertainties for the experimentally determined quantities in this study are as follows: between 3% and 6.5% for burning velocity; between 1% and 4.5% for normalized burning velocity (the *normalized* burning velocity is defined as the burning velocity of the inhibited flame divided by the burning velocity of the uninhibited flame, which can be found in Table 1); 6.5% for  $\text{Fe}(\text{CO})_5$  mole fraction; 1.4% for equivalence ratio; 1.1% for oxygen mole fraction; and 1.2% for hydrogen mole fraction in the reactants. For the scattering measurements, the combination of slight fluctuations in the flame position, small particle scattering cross section, steep spatial gradients in the flame, and system noise cause the scattering signal to vary about a local mean value at any given location. The expanded relative uncertainty of the  $Q_{vv}$  is no

more than 10% of the mean in the particle zone and no more than 20% of the mean in the unburned reactants.

## RESULTS AND DISCUSSION

### *CH<sub>4</sub> Flames*

Addition of iron pentacarbonyl to the premixed flame leads to a two-zone structure for particle formation; Figure 2 shows the scattering cross section  $Q_{vv}$  as a function of the radial distance  $r$  from the centerline for measurements at a height of 7 mm in a CH<sub>4</sub>-air flame with 200 ppm of Fe(CO)<sub>5</sub>. As the figure shows, the particles far outside the main reaction zone of the flame ( $|r| > 7$  mm) have a scattering signal which is three orders of magnitude larger than the in-flame particles (the signals were collected separately at different amplifier gains).

In Figure 2, particles are seen to form in the main reaction zone of the flame ( $|r| \approx 2-3$  mm), yielding a peak scattering signal a few times higher than that of the Rayleigh scattering by the cold reactants (the signal at  $r=0$ ). These particles disappear outside the main reaction zone of the flame ( $|r| > 4$  mm), and far beyond that ( $|r| > 7$  mm), particles form with a enormous scattering cross section. Although the shroud flow around the burner (5 L/min) probably reduces the particle formation (through dilution), the low gas velocity and low temperature in the outer annulus may cause the increase in the particle scattering cross section, and it is also possible that mature particles are circulating near the edges of the chimney. A consequence of the high scattering in the outer annulus is that it is impractical to make a measurement of the

laser extinction through the area of interest (the premixed flame between  $-7 \text{ mm} < r < 7 \text{ mm}$ ). The total laser extinction through the chimney is about 1%, and that is dominated by the outer annulus, which is the post-combustion region of the flame and does not affect flame propagation. Because of the disparate scattering signal strengths in the two regions of the flame, the usual tomographic reconstruction techniques are impractical. Nonetheless, in the absence of laser extinction data, it is possible to use the small *scattering* signal in the flame zone ( $|r| > 5 \text{ mm}$ ) to study particulate formation.

It is worthwhile to discuss the flame structure of the present premixed flame. While there exists a two-zone structure for *particle formation*, as shown in Figure 2, there are not two reaction zones in the flame because, unlike partially premixed flames, the present flames have  $\phi=1.0$  based on the primary gases. We have confirmed the single reaction zone structure (in tests without added  $\text{Fe}(\text{CO})_5$ ) through examination of the Rayleigh scattering results, previous thermocouple temperature data [55], and tests with nitrogen co-flow (instead of air).

In the following discussions, the particle scattering signal at varying radii and a fixed height above the burner are presented. With the present nozzle burner, streamlines *within* the flame are vertical, and parallel. As has been discussed thoroughly in the literature [56], the gases expand in the flame, causing the flow streamlines to gain a radial component of velocity and diverge outward. At central heights in the flame and just *outside* of the region of visible emission, it is found that the streamlines make an angle of about  $45^\circ$  to the horizontal, and they are nearly parallel. Hence, at a fixed height above the burner, increasing radial positions beyond the flame

correspond to larger distances and times since passage through the flame. Although measurements at different radii correspond to different streamlines, the time-temperature history of adjacent streamlines is sufficiently similar so that they can be assumed to be equivalent, and increasing the radius can be thought of as increasing time or distance from the main reaction zone.

In order to determine how particle formation depends on  $\text{Fe}(\text{CO})_5$  concentration, we measured radial profiles of the scattering signal for varying  $\text{Fe}(\text{CO})_5$  mole fractions ( $X_{in}$ ) at a height of 7 mm above the burner rim (Figure 3). Referring to Figure 3,  $r = 0$  corresponds to the centerline of the conical Bunsen-type flame. At this flame height (7 mm), cold reactants are in the region of  $|r| < 2$  mm, the primary reaction zone of the flame extends from  $|r| \approx 2$  to 3 mm, and the hot combustion products are in the region of  $|r| > 3$  mm. The figure shows that with 50 ppm of  $\text{Fe}(\text{CO})_5$ ,  $Q_{vv}$  is only slightly higher than that of the uninhibited flame; whereas above that value, significant peaks in  $Q_{vv}$  appear in the flame zone, indicating particle formation. Note that the scattering cross section of the particles at 300 ppm is only 20 times that of room air, which implies very small diameters or number densities. The existence of sharp peaks in Figure 3, as opposed to a step function, may be explained as follows: in the reaction zone ( $|r| \approx 2$  mm), the  $\text{Fe}(\text{CO})_5$  decomposes, resulting in supersaturated vapor of iron-containing intermediates (the gas-phase inhibiting species). If the mole fraction of these species is high enough, nucleation and particle growth occurs. As the particles are heated by the flame ( $|r| > 3$  mm), they evaporate, and their scattering cross section is reduced. Far downstream of the flame, the long residence times and cooler gases cause the formation

of stable iron oxide particles (seen as the very large scattering signals at  $|r| > 7$  mm in Figure 2) which persist (and coat the chimney and exhaust system).

We expect that the particle profiles are relatively unaffected by thermophoresis – a process in which particles drift down a temperature gradient – because calculations (based on Refs. [57,58]) show that the thermophoretic velocity is never more than one-quarter the gas velocity at any point in the flame zone.

Previous experimental results [6,10] show that the burning velocity starts to level off at an  $\text{Fe}(\text{CO})_5$  mole fraction of about 100 ppm. It has been suggested that this is due to condensation of the active iron-containing inhibiting species as they reach their saturation vapor pressure. Further, for flames at higher oxygen mole fraction (i.e. higher temperature), the leveling-off point shifts to a higher value of  $X_{in}$ . A reasonable explanation is that at higher temperature, higher concentrations of iron can remain in the gas phase before condensation occurs. Increasing the oxygen mole fraction in the air ( $X_{O_2,ox}$ ) from 0.21 to 0.24 provides a 130 K increase in adiabatic flame temperature (see Table 1). The scattering results (not shown) for higher temperature  $\text{CH}_4$  flames ( $X_{O_2,ox} = 0.24$ ) have similar shape and dependence on  $X_{in}$  as those for  $X_{O_2,ox} = 0.21$ , but the measured  $Q_{vv}$ 's are between 2 and 4 times lower, implying fewer or smaller particles.

The ultimate goal of these experiments is to determine the effect of particles on flame inhibition by  $\text{Fe}(\text{CO})_5$ . Ideally, the particles formed from the  $\text{Fe}(\text{CO})_5$  precursor would be quantified by measuring their size, number density, volume fraction and number of molecules per particle, but at this point such data are unavailable. In their

absence, the  $Q_{vv}$  data shown in Figure 3 and those for  $X_{O_2,ox} = 0.24$  can be used as qualitative measures of the particle loading at a given inhibitor mole fraction.

Evidence that particle formation leads to the decrease in inhibitor effectiveness is found in Figure 4, which shows the peak  $Q_{vv}$  along with the normalized burning velocity at various inhibitor concentrations. At low  $X_{in}$ , where the inhibition is believed to be primarily a gas-phase effect, the burning velocity depends strongly on  $Fe(CO)_5$  concentration, and the  $Q_{vv}$  is relatively small. For either value of  $X_{O_2,ox}$ , there exists an  $Fe(CO)_5$  mole fraction at which the marginal inhibition becomes much smaller (approximately 100 ppm for  $X_{O_2,ox} = 0.21$  and 300 ppm for  $X_{O_2,ox} = 0.24$ ). At these values (especially for  $X_{O_2,ox} = 0.21$ ), the peak scattering cross sections rise sharply. Thus, it appears that a decrease in inhibitor effectiveness is correlated with particle formation, supporting the previous proposal that condensation of iron containing species weakens the inhibitor efficiency. It is also noteworthy that for the flames with  $X_{O_2,ox} = 0.24$ , the inhibition continues to a higher value of  $X_{in}$  and the scattering signal is always smaller than for flames with  $X_{O_2,ox} = 0.21$ . The higher flame temperatures with  $X_{O_2,ox} = 0.24$  may be the reason for the decreased  $Q_{vv}$ , but the higher burning velocity of these flames (see Table 1) also yield a shorter residence time for particle growth, complicating the interpretation. Other techniques of changing flame temperature in  $CH_4$  flames, such as replacing some of the nitrogen with argon, also result in simultaneous change in burning velocity. Alternatively, as will be described in the next section, CO flames with

varying amounts of H<sub>2</sub> can provide flames with different burning velocities without appreciably changing the adiabatic flame temperature.

### *Carbon Monoxide Flames*

Stoichiometric CO flames with hydrogen mole fraction ( $X_{H_2}$ ) of 0.005, 0.01, and 0.015, and elevated oxygen content relative to air ( $X_{O_2,ox} = 0.24$ ), have burning velocities between 35 and 60 cm/s and adiabatic flame temperatures near 2470 K (see Table 1). Measurements of scattering cross section in each flame at various values of  $X_{in}$  can provide information about the relative importance of peak flame temperature and residence time.

The scattering results for the CO-H<sub>2</sub> flames are qualitatively similar to those for the CH<sub>4</sub> flames of Figure 3: the scattering increases with increasing  $X_{in}$ , and the particles appear and then disappear. A difference, however, is that for the CO flames at high Fe(CO)<sub>5</sub> loading and low H<sub>2</sub> content, each of the two  $Q_{vv}$  peaks has a twin-lobed structure. These structures may be due to variations in the refractive index as the particles change composition, or due to thermophoretic size segregation effects, as described by Zachariah et al. [59].

Following the procedure used for the CH<sub>4</sub> flames, we correlate the scattering data for the CO flames with the inhibition by Fe(CO)<sub>5</sub> by plotting the peak  $Q_{vv}$  values and normalized burning velocity [9] for each flame condition in Figure 5. As was seen for CH<sub>4</sub> flames, the peak  $Q_{vv}$  is relatively small at low  $X_{in}$  where the inhibition effect is

strongest, and rises sharply as  $X_{in}$  increases. Comparing the values of  $X_{in}$  at which the normalized burning velocity curves level off, we see that the 0.5% H<sub>2</sub> curve levels off first, followed by the 1.0% H<sub>2</sub> and then the 1.5% H<sub>2</sub>. The data in Figure 5 support the claim that particles reduce the inhibition effect: higher scattering signals correspond to greater loss of effectiveness (i.e., leveling off in the burning velocity curves). The three flames in Figure 5 have roughly the same adiabatic flame temperature but very different peak scattering cross sections with added Fe(CO)<sub>5</sub>. These results can be used with those of the CH<sub>4</sub> flames at varying  $X_{O_2,ox}$  to show the importance of residence time for particle formation.

Figure 6 shows the maximum value of  $Q_{vv}$  as a function of burning velocity (which is inversely related to residence time) for a variety of flames at three values of the inhibitor loading. The figure presents data for CH<sub>4</sub> flames (open symbols) at low (l) and medium (m) temperature, and for CO flames (closed symbols) at high (h) temperature. The three values of Fe(CO)<sub>5</sub> loading, 100, 200, and 300 ppm are indicated by circles, diamonds, and squares, respectively. While eight parameters are shown in the figure, the peak value of  $Q_{vv}$  for a given inhibitor loading is found to depend most strongly upon the burning velocity (i.e. the residence time). The linear dependence becomes strongest at 300 ppm inhibitor, in which case a doubling of the burning velocity (halving of residence time) yields a four-fold decrease in maximum  $Q_{vv}$ . These results clearly illustrate the importance of residence time in particle formation; a similar analysis using adiabatic flame temperature as the independent variable shows no significant correlation.

## *Particle Size and Morphology*

Although exact laser-based measurements of the particle size and number density are not practical in the present nozzle burner premixed flames (because of the two-zone structure shown in Figure 2), we can make estimates of particle properties and use extractive sampling to obtain information about the particles. The information from these techniques can be used to provide insight into particle behavior in the premixed flames, and provide input for a heterogeneous inhibition model.

We can obtain an upper limit for particle properties by estimating the fraction of that iron condenses, calculating the resulting extinction coefficient, and combining it with the scattering data to predict a range of possible particle sizes and number densities. The mass concentration of iron particles ( $\text{g}/\text{cm}^3$ ) is  $[P] = f_c X_{in} N_{gas} M_P / N_A$ , where  $f_c$  is the fraction of the iron that has condensed,  $N_{gas}$  is the number density of the gas,  $M_P$  is the molecular mass of the particulate material, and  $N_A$  is Avogadro's number. The volume fraction ( $f_v$ ) can be calculated as  $f_v = [P] / \rho_{P(s)}$ , where  $\rho_{P(s)}$  is the density of the solid particle material. The extinction coefficient can then be calculated with  $k_{ext} = 6\pi E(\tilde{m}) f_v / \lambda$  [48]. Finally, we use the equations for monodisperse Rayleigh

scatterers to obtain  $D = \left[ \frac{Q_{vv}}{k_{ext}} \frac{E(\tilde{m})}{F(\tilde{m})} \left( \frac{4\lambda^3}{\pi^2} \right) \right]^{1/3}$ , and  $N = \frac{\lambda k_{ext}}{\pi^2 E(\tilde{m}) D^3}$ .

We present calculated particle properties for  $f_c = 0.5$  and  $1.0$  (50% and 100% condensation). A comparison between numerically calculated inhibition assuming no condensation and the measured inhibition at 200 ppm implies that 50% of the FeO has

condensed, while considering 100% condensation provides an upper limit. We use the approach outlined above with the peak scattering data (at a height of 7 mm) from Figure 3. We calculate the properties for particles formed in CH<sub>4</sub>/air flame with  $X_{in} = 200$  ppm, estimating from the  $Q_{vv}$  data that the peak scattering cross section occurs at 1500 K and assuming that the particle material is FeO ( $\rho_{P(s)} = 5.7$  g/cm<sup>3</sup> [60]). At such conditions, for  $f_c = 0.5$  and 1.0, the particles have a volume fractions of  $1.2 \times 10^{-8}$  and  $2.2 \times 10^{-8}$ , diameters of 16 nm and 13 nm, and number density of  $5.3 \times 10^9$  cm<sup>-3</sup> and  $2.1 \times 10^{10}$  cm<sup>-3</sup>. Using the optical and bulk properties of Fe instead of FeO increases the inferred diameter by 15% and the number density by 9%. While it is possible that the particles also contain combinations of iron compounds and carbonaceous material from soot, we consider it unlikely since the flames are not fuel-rich, and we did not observe any evidence of soot from the scattering measurements in uninhibited flames.

Thermophoretic sampling allows measurement of particles at the present flame conditions. Using the rapid sampling technique, we collected samples at various flame conditions at a height of 7 mm above the burner rim, at a radial position corresponding to approximate center of the main reaction zone ( $r = 2.7 \pm 0.3$  mm). The image shown in Figure 7 corresponds to a dwell time of 375 ms in a flame with  $X_{in} = 200$  ppm. The particles show a moderate degree of agglomeration, with about 1 to 10 primary particles per agglomerate and primary particle sizes of under 20 nm. Contamination of the grid by particles from outside the premixed flame zone is possible, and may account for the large number of agglomerates in the image. The primary particle diameters estimated above from the scattering signal with assumed amounts of iron condensation, and from

the TEM images in Figure 7 are in reasonable agreement. These small diameters, 10 to 20 nm, support the possibility of particles evaporating as they convect to regions of higher temperature.

### *Perfect Heterogeneous Inhibition Model*

There have been conflicting claims in the literature as to whether inhibition by  $\text{Fe}(\text{CO})_5$  is a gas-phase or heterogeneous effect [1-5]. A heterogeneous inhibition mechanism is reasonable since iron and iron oxides are used in various industrial processes as heterogeneous catalysts. It is unclear, however, if the same catalytic behavior occurs on the nanoparticles found in the present flames. Preining [61] has argued that particles with diameters on the order of 5 nm behave like neither the gas phase nor the bulk phase because of the interactions between the electronic structures of the molecules in the particle. Although Preining's contention does not rule out the possibility of catalytic activity, it implies that the catalytic properties of the bulk phase may not be reproduced in nanoparticles, and further study is required to determine the catalytic properties of the nanoparticles. Although it is too early to completely disregard the possibility of heterogeneous inhibition, the experimental data in Figure 4 suggest that the inhibition is primarily gas-phase. If the inhibition chemistry were primarily heterogeneous, we would expect the maximum particle scattering to be high for  $\text{Fe}(\text{CO})_5$  mole fraction below 200 ppm – when the marginal inhibition is strongest – and leveling-off above 200 ppm.

Lacking direct measurements of heterogeneous chemical effects, it is of interest to estimate the maximum possible effect of surface inhibition and to determine if heterogeneous chemistry can reproduce the performance of  $\text{Fe}(\text{CO})_5$  under idealized conditions. A model of heterogeneous radical recombination was presented by Baratov et al. [62] for larger particles (ca. 5  $\mu\text{m}$ ) with the goal of understanding powdered fire suppressants such as sodium bicarbonate. Additionally, Jensen and Webb [4] simulated catalytic radical recombination by metal additives in a rocket plume and found that condensed-phase additives had a smaller effect than gas-phase additives. The work of Babushok et al. [7], who developed a chemical mechanism for an ideal inhibitor which catalytically scavenges radicals at gas-kinetic rates, serves as an inspiration for the present model.

The present model seeks to determine the maximum reaction rates between particles and radicals. For simplicity, we assume a two-step heterogeneous inhibition mechanism (Langmuir-Rideal type) which is initiated by the adsorption of a radical  $\text{R}$  onto a particle surface  $\text{P}$ :  $\text{R} + \text{P} \rightarrow \text{RP}$ . This reaction is followed by the reaction of the activated particle  $\text{RP}$  with a radical, and desorption of the recombined radicals  $\text{R}_2$ :  $\text{RP} + \text{R} \rightarrow \text{R}_2 + \text{P}$ . A number of other important assumptions are made: 1) all of the gaseous inhibitor immediately becomes particulate matter, 2) the particles are spherical with a specified log-normal diameter distribution [63-65] which is unchanged through the flame, 3) every collision of a radical with a particle results in adsorption and every collision of a radical with an activated particle results in reaction and desorption, and 4) only H-atom recombination is considered, since numerical results show that the iron

species primarily scavenge H atoms (note that the additional effect of adding O and OH recombination would be minor). Many other effects are not considered, such as multiple adsorption sites on particles, non-unity adsorption probabilities, steric factors, and saturation of the surface sites; all of these would reduce the efficiency of the radical recombination on the particle surface.

For compatibility with the Chemkin codes used here, we calculate an “effective mole fraction” of particles which can be directly entered into the *Premix* [66] input file and maintains the proper units for the calculation. The approximation for the effective mole fraction is

$$X_p = \frac{\text{Number density of particles}}{\text{Number density of all gaseous reactants}} = \frac{X_{in} N_o / \int_0^{\infty} n(r) f(r) d(\ln r)}{N_o},$$

where  $N_o$  is the number density of the reactant gas,  $n(r)$  is the number of iron atoms in a particle of radius  $r$ , and  $f(r)$  is the probability density function of the lognormal distribution. The numerator expresses the number density of the particles as the ratio of the number density of inhibitor molecules ( $X_{in} N_o$ ) to the average number of molecules per particle. The number of iron atoms per particle ( $n(r) = 58.607 r^{3.5478}$ ) is calculated from the curve fit of results of Jensen [67], which assume hard sphere packing and a decrease in packing density for particles with a diameter less than 10 nm.

The reaction rates between radicals and particles are calculated using kinetic theory, assuming that the particles are in the free molecular regime. The collision rate

between an atom and particle is  $k = d_{RP}^2 \left( \frac{8\pi k_B}{\mu_{RP}} \right)^{1/2} N_A T^{1/2}$ , where  $d_{RP}$  is the collision

diameter of the radical and particle ( $d_R + d_P$ ),  $k_B$  is Boltzmann's constant, and  $\mu_{RP}$  is the reduced mass of the two bodies ( $m_{RM} / (m_R + m_P)$ ). Molecular masses and diameters are taken from Ref. [68]. Numerical experiments show that variation of the thermodynamic and transport properties of the particles has no appreciable impact on the results for burning velocity.

Calculated values of the pre-exponential and effective mole fraction are listed in Table 2. The conversion of gas to particles results in two changes to the overall reactivity: a reduction in the effective mole fraction of the inhibiting species (between  $10^{-4}$  and  $10^{-6}$  times smaller) because of more inhibitor atoms per particle, and an increase in the rate constant ( $10^3$  to  $10^5$  times the gas kinetic rate for a single molecule) because of the larger cross sectional area of the particles relative to molecules. Figure 8 shows the normalized burning velocity as a function of  $X_{in}$  for mean particle diameters of 10 nm, 20 nm, 40 nm and 80 nm. Since the number of particles scales as  $1/d_m^3$ , while the pre-exponential scales as  $1/d_m^2$ , the smaller particles are more effective. The inhibition effect of this idealized inhibitor is significant, but not nearly as strong as that of  $\text{Fe}(\text{CO})_5$  or the perfect homogeneous inhibitor. These idealized calculations support the proposals [5,7] that only gas-phase chemistry is fast enough to account for the extraordinary inhibition effect of  $\text{Fe}(\text{CO})_5$ , since a more realistic model of heterogeneous radical recombination would probably result in less inhibition. It is interesting to note that the residual inhibition of  $\text{Fe}(\text{CO})_5$  at  $X_{in} > 300$  ppm, while small compared to values at  $X_{in} < 100$

ppm, is not zero. It is, in fact, comparable to agents such as  $\text{CF}_3\text{Br}$  and may be due to heterogeneous inhibition.

## CONCLUSIONS

Laser light scattering has been used to investigate particle formation in  $\text{Fe}(\text{CO})_5$ -inhibited premixed flames. Particles form early in the flame zone, nucleate and grow to a peak scattering cross section, then disappear as the temperature increases to the flame temperature; far downstream in the post-combustion gases, the peak scattering signal is several orders of magnitude larger than the peak value near the main reaction zone of the flame. Thermophoretic sampling as well as estimates of the size from inhibitor loading and scattering signal show particles with diameters between 10 and 30 nm.

Experimental results support the hypothesis that condensation reduces the inhibition. The  $\text{Fe}(\text{CO})_5$  mole fraction at which the normalized burning velocity levels off corresponds to the mole fraction at which the in-flame particle scattering cross section begins to sharply increase. Measurements in three  $\text{CO-H}_2$  flames with similar adiabatic flame temperatures but different burning velocities demonstrate the importance of residence time for particle formation in premixed flames, as the highest scattering signals occur in flames with the lowest burning velocity. The experimental results also imply that heterogeneous chemical effects are small since the particles appear at  $X_{in}$  where inhibition effects are weak. In addition, an idealized model shows that heterogeneous chemistry alone can not account for the inhibition exhibited by  $\text{Fe}(\text{CO})_5$  for particle diameters of 10 nm and larger. For particles of diameter much less

than 10 nm, however, the possibility that they contribute to the inhibition cannot be ruled out.

Particle dynamics may affect the performance of ultra-effective fire suppressants in practice and it is important to understand the effects. For example, if the residence time is low enough, significant condensation of active species and the subsequent reduction in effectiveness may not occur. In situations with long particle formation residence times, it may be possible to reduce the undesired loss of effectiveness due to condensation by using several compounds together (with non-condensing amounts of each), or by selecting compounds with a high vapor pressure condensed phase.

Further experiments on particle formation in premixed  $\text{Fe}(\text{CO})_5$ -inhibited flames would benefit from a one-dimensional flame with a longer path length for the scattering and extinction techniques. In addition, a direct measurement of the catalytic effect of iron-containing nanoparticles may allow determination of the role of heterogeneous chemistry in flame inhibition by  $\text{Fe}(\text{CO})_5$ .

## ACKNOWLEDGEMENT

*The authors thank undergraduate student intern Nikki Prive for assistance with data acquisition and uncertainty analysis programs and Maria Aquino for operating the electron microscope and advising us on sampling techniques. Discussions with Dr. George Mulholland about particle measurement techniques, Dr. Viet Nguyen about beam steering, and Dr. Valeri Babushok about the heterogeneous inhibitor model contributed greatly to this work.*

## REFERENCES

- [1]. Lask, G. and Wagner, H.G., *Proceedings of the Combustion Institute, Vol. 8*, Williams and Wilkins Co., Baltimore, 1962, pp. 432-438.
- [2]. Bonne, U., Jost, W., and Wagner, H.G., *Fire Research Abstracts and Reviews* 4:6 (1962).
- [3]. Fristrom, R.M. and Sawyer, R.F., *AGARD Conference on Aircraft Fuels, Lubricants, and Fire Safety, AGARD-CP 84-71*, 1971, pp.
- [4]. Jensen, D.E. and Webb, B.C., *AIAA Journal* 14:947 (1976).
- [5]. Rumminger, M.D., Reinelt, D., Babushok, V., and Linteris, G.T., *Combust. Flame* 116:207 (1999).
- [6]. Reinelt, D. and Linteris, G.T., *Proceedings of the Combustion Institute, Vol. 26*, The Combustion Institute, Pittsburgh, PA, 1996, pp. 1421-1428.
- [7]. Babushok, V., Tsang, W., Linteris, G.T., and Reinelt, D., *Combust. Flame* 115:551 (1998).
- [8]. Rumminger, M.D. and Linteris, G.T., *Combust. Flame* 120:451 (2000).
- [9]. Rumminger, M. D. and Linteris, G. T., *Inhibition of Premixed Carbon Monoxide-Hydrogen-Oxygen-Nitrogen Flames by Iron Pentacarbonyl*, National Institute of Standards and Technology, NIST IR 6360, 1999.
- [10]. Rumminger, M.D., Reinelt, D., Babushok, V., and Linteris, G.T., *Halon Options Technical Working Conference*, Albuquerque, NM, 1998, pp. 145-156.
- [11]. Rumminger M.D. and Linteris, G.T., "Numerical Modeling of Counterflow Diffusion Flames Inhibited by Iron Pentacarbonyl", to appear in the *Sixth International Symposium on Fire Safety Science* July 1999.
- [12]. Kung, R.T.V. and Bauer, S.H., *Proceedings of the Eighth International Shock Tube Symposium*, 1971, pp. 61-1-61/20.
- [13]. Vlasov, P.A., Karasevich, Y.K., and Smirnov, V.N., *High Temperature* 35:198 (1997).
- [14]. Vlasov, P.A., Zaslono, I.S., and Karasevich, Y.K., *High Temperature* 36:189 (1998).
- [15]. Vlasov, P.A., Zaslono, I.S., and Karasevich, Y.K., *High Temperature* 33:76 (1995).
- [16]. Vlasov, P.A., Zaslono, I.S., Karasevich, Y.K., and Lidskii, B.V., *High Temperature* 35:934 (1997).
- [17]. Hurst, S.M. and Bauer, S.H., *Rev. Sci. Instrum.* 64:1342 (1993).
- [18]. Krestinin, A.V., Smirnov, V.N., and Zaslono, I.S., *Khimicheskaya Fizika (Chemical Physics)* 9:418 (1990).
- [19]. Insepov, Z.A., Karatajev, E.M., and Norman, G.E., *Zeitschrift Fur Physik D-Atoms Molecules and Clusters* 20:449 (1991).
- [20]. Frurip, D.J. and Bauer, S.H., *J. Phys. Chem.* 81:1001 (1977).
- [21]. Freund, H.J. and Bauer, S.H., *J. Phys. Chem.* 81:994 (1977).
- [22]. Bonczyk, P.A., *Combust. Flame* 87:233 (1991).
- [23]. Kasper, M., Sattler, K., Siegmann, K., Matter, U., and Siegmann, H.C., *J. Aerosol Sci.* 30:217 (1999).
- [24]. Kasper, M. and Siegmann, K., *Combust. Sci. Technol.* 140:333 (1998).

- [25]. Mitchell, J.B.A., *Combust. Flame* 86:179 (1991).
- [26]. Zhang, J. and Megaridis, C.M., *Combust. Flame* 105:528 (1996).
- [27]. Zhang, J. and Megaridis, C.M., *Proceedings of the Combustion Institute, Vol. 25*, The Combustion Institute, Pittsburgh, 1994, pp. 593-600.
- [28]. Wallis, D.J., Browning, N.D., Megaridis, C.M., and Nellist, P.D., *Journal of Microscopy-Oxford* 184:185 (1996).
- [29]. Feitelberg, A.S., Longwell, J.P., and Sarofim, A.F., *Combust. Flame* 92:241 (1993).
- [30]. Hahn, D.W. and Charalampopoulos, T.T., *J. Phys. D: Appl. Phys.* 26:1851 (1993).
- [31]. Hahn, D. W., Ph.D. Dissertation, Louisiana State University, 1992.
- [32]. Ritrievi, K.E., Longwell, J.P., and Sarofim, A.F., *Combust. Flame* 70:17 (1987).
- [33]. Somasundaram, G. and Sunavala, P.D., *Fuel* 68:921 (1989).
- [34]. Tanke, D., Wagner, H.G., and Zaslonko, I.S., *Proceedings of the Combustion Institute, Vol. 27*, The Combustion Institute, Pittsburgh, 1998, pp. 1597-1604.
- [35]. Starikovskiy, A.Y., Thienel, T., Wagner, H.G., and Zaslonko, I.S., *Berichte Der Bunsen-Gesellschaft-Physical Chemistry Chemical Physics* 102:1815 (1998).
- [36]. Biswas, P., Wu, C.Y., Zachariah, M.R., and Mcmillin, B., *J. Mater. Res.* 12:714 (1997).
- [37]. Park, K.Y., Jang, H.D., and Choi, C.S., *Aerosol Science and Technology* 28:215 (1998).
- [38]. Park, K.Y. and Jeong, H.J., *Korean Journal of Chemical Engineering* 16:64 (1999).
- [39]. Girshick, S.L., Chiu, C.P., Muno, R., Wu, C.Y., Yang, L., Singh, S.K., and Mcmurry, P.H., *J. Aerosol Sci.* 24:367 (1993).
- [40]. Fu, T.H., Cheng, M.T., Wong, F.C.H., and Shaw, D.T., *Aerosol Science and Technology* 15:19 (1991).
- [41]. McMillin, B.K., Biswas, P., and Zachariah, M.R., *J. Mater. Res.* 11:1552 (1996).
- [42]. Zachariah, M.R., Aquino, M.I., Shull, R.D., and Steel, E.B., *Nanostructured Materials* 5:383 (1995).
- [43]. Zhang, Z. and Charalampopoulos, T.T., *Proceedings of the Combustion Institute, Vol. 26*, The Combustion Institute, Pittsburgh, 1996, pp. 1851-1858.
- [44]. Linteris, G.T. and Truett, L., *Combust. Flame* 106:15 (1996).
- [45]. Mache, H. and Hebra, A., *Sitzungsber. Österreich. Akad. Wiss. Ila*, 150:157 (1941).
- [46]. Gilbert, A.G. and Sulzmann, K.G.P., *J. Electrochem. Soc.* 121:832 (1974).
- [47]. Charalampopoulos, T.T., Hahn, D.W., and Chang, H., *Appl. Opt.* 31:6519 (1992).
- [48]. Santoro, R.J., Semerjian, H.G., and Dobbins, R.A., *Combust. Flame* 51:203 (1983).
- [49]. Nguyen, Q.-V., Ph.D. Dissertation, University of California, Berkeley, 1995.
- [50]. Dibble, R. W., Ph.D. Dissertation, University of Wisconsin, Madison, 1975.
- [51]. D'Alessio, A., in *Particulate Carbon: Formation during Combustion* (Siegla, D. C. and Smith, G. W., Ed.), Plenum Press, New York, pp. 207-256, 1981.
- [52]. Dobbins, R.A. and Megaridis, C.M., *Langmuir* 3:254 (1987).
- [53]. Koylu, U.O., Mcenally, C.S., Rosner, D.E., and Pfefferle, L.D., *Combust. Flame* 110:494 (1997).
- [54]. Taylor, B. N. and Kuyatt, C. E., *Guidelines for Evaluating and Expressing the Uncertainty of NIST Measurement Results*, National Institute of Standards and Technology, NIST Technical Note 1297, 1994.

- [55]. Linteris, G. T., in *Halon Replacements* (A.W. Miziolek and W. Tsang, Ed.), ACS Symposium Series 611, American Chemical Society, Washington, DC, pp. 260-274, 1995.
- [56]. Lewis, B. and von Elbe, G., *Combustion, Flames and Explosions*, Academic, New York, 1987.
- [57]. Waldmann, L. and Schmidt, K. H., in *Aerosol Science* (C.N. Davies, Ed.), Academic Press, New York, pp. 137-162, 1966.
- [58]. Talbot, L., Cheng, R.K., Schefer, R.W., and Willis, D.R., *J. Fluid Mech.* 101:737 (1980).
- [59]. Zachariah, M.R., Chin, D., Semerjian, H.G., and Katz, J.L., *Combust. Flame* 78:287 (1989).
- [60]. R.C. Weast, *Handbook of Chemistry and Physics* B-103 (1975).
- [61]. Preining, O., *J. Aerosol Sci.* 29:481 (1998).
- [62]. Baratov, A.N., Dobrikov, V.V., and Shamonin, V.G., *Proceedings of IX All Union Symposium on Combustion and Explosions*, (in Russian), Institute of Chemical Physics, Chernogolovka, 1989, pp. 37-40.
- [63]. Granqvist, C.G. and Buhrman, R.A., *J. Appl. Phys.* 47:2200 (1976).
- [64]. Xing, Y.C., Koylu, U.O., and Rosner, D.E., *Combust. Flame* 107:85 (1996).
- [65]. Hahn, D.W. and Charalampopoulos, T.T., *Proceedings of the Combustion Institute, Vol. 24*, The Combustion Institute, Pittsburgh, 1992, pp. 1007-1014.
- [66]. Kee, R. J., Grcar, J. F., Smooke, M. D., and Miller, J. A., *A Fortran Computer Program for Modeling Steady Laminar One-dimensional Premixed Flames*, Sandia National Laboratories Report, SAND85-8240, 1991.
- [67]. Jensen, D.E., *J. Chem. Soc., Faraday Trans.* 76:1494 (1980).
- [68]. Karplus, M. and Porter, R. N., *Atoms & Molecules*, Benjamin, Menlo Park, CA, 1970.

## TABLE AND FIGURE CAPTIONS

Table 1: Oxygen content of 'air,' mole fraction of hydrogen in reactants, measured burning velocity, and calculated maximum temperature of the uninhibited stoichiometric flames used in this paper. CH<sub>4</sub> data from Ref. [6], CO-H<sub>2</sub> data from Ref. [8].

Table 2: Representative properties of perfect heterogeneous inhibitor with 100 ppm of precursor.

Figure 1: Schematic of laser scattering/extinction system: C, chopper; M, mirror; G, beam pick-off; L, lens; S, spatial filter (circular aperture); Po, polarizer; F, laser-line and neutral density filters; PMT, photomultiplier; P, pinhole; IS, integrating sphere. (Note: Some structural components are not shown, and the drawing is not to scale.)

Figure 2: Scattering cross section  $Q_{vv}$  as a function of the radial distance  $r$  from the burner centerline at 7 mm height in stoichiometric CH<sub>4</sub>-air flame with 200 ppm of Fe(CO)<sub>5</sub>.

Figure 3: Measured scattering cross section through a stoichiometric CH<sub>4</sub>-air flame 7 mm above the burner rim at various inhibitor mole fractions.

Figure 4: Normalized burning velocity (from Ref. [6]) and maximum  $Q_{vv}$  for  $\phi=1.0$  CH<sub>4</sub> flame with  $X_{O_2,ox} = 0.21$  and  $0.24$ .

Figure 5: Maximum scattering signal and normalized burning velocity (from Ref.[8]) for CO-H<sub>2</sub> flames as Fe(CO)<sub>5</sub> concentration varies.

Figure 6: Maximum  $Q_{vv}$  for flames of CH<sub>4</sub> (open symbols) and CO (closed symbols) as a function of the burning velocity (from Ref. [6] and [8]). The letters correspond to the adiabatic flame temperature (l,m,h: low, medium, and high, 2220, 2350, and 2470 K), while the symbol shape (square, diamond, and circle) corresponds to the loading of Fe(CO)<sub>5</sub>: 100 ppm , 200 ppm , and 300 ppm .

Figure 7 : Electron microscope picture of particles sampled from a CH<sub>4</sub>/air premixed flame with  $X_{in} = 200$  ppm.

Figure 8: Calculated normalized burning velocity for several diameters  $d_m$  of ideal heterogeneous inhibitor. Also shown are Fe(CO)<sub>5</sub> data [6], and calculated normalized burning velocity using the perfect gas-phase inhibitor mechanism [7].

**Table 1: Oxygen content of ‘air,’ mole fraction of hydrogen in reactants, measured burning velocity, and calculated maximum temperature of the uninhibited stoichiometric flames used in this paper. CH<sub>4</sub> data from Ref. [6], CO-H<sub>2</sub> data from Ref. [8].**

Fuel	$X_{O_2,ox}$	$X_{H_2}$	$v_{o,exp}$ (cm/s)	$T_{max,num}$ (K)
CH <sub>4</sub>	0.21	0	40.6 ± 2.0	2224
	0.24	0	59.2 ± 3.0	2353
CO-H <sub>2</sub>	0.21	0.01	39.2 ± 1.1	2376
	0.24	0.005	36.2 ± 0.9	2468
	0.24	0.01	46.2 ± 1.4	2471
	0.24	0.015	59.0 ± 2.4	2475

**Table 2: Representative properties of perfect heterogeneous inhibitor with 100 ppm of precursor.**

Mean Diameter (nm)	A (cm <sup>3</sup> /mol-s- K <sup>1/2</sup> ) H+P→HP HP+H→H <sub>2</sub>	Effective Mole Fraction of Particles	Number Density of Particles (cm <sup>-3</sup> )	Average atoms per particle
10	3.22E+16	1.84E-08	4.96E+11	5.43E+03
20	1.28E+17	2.95E-09	7.93E+10	3.39E+04
40	5.12E+17	4.72E-10	1.27E+10	2.12E+05
80	2.05E+18	7.55E-11	2.03E+09	1.32E+06

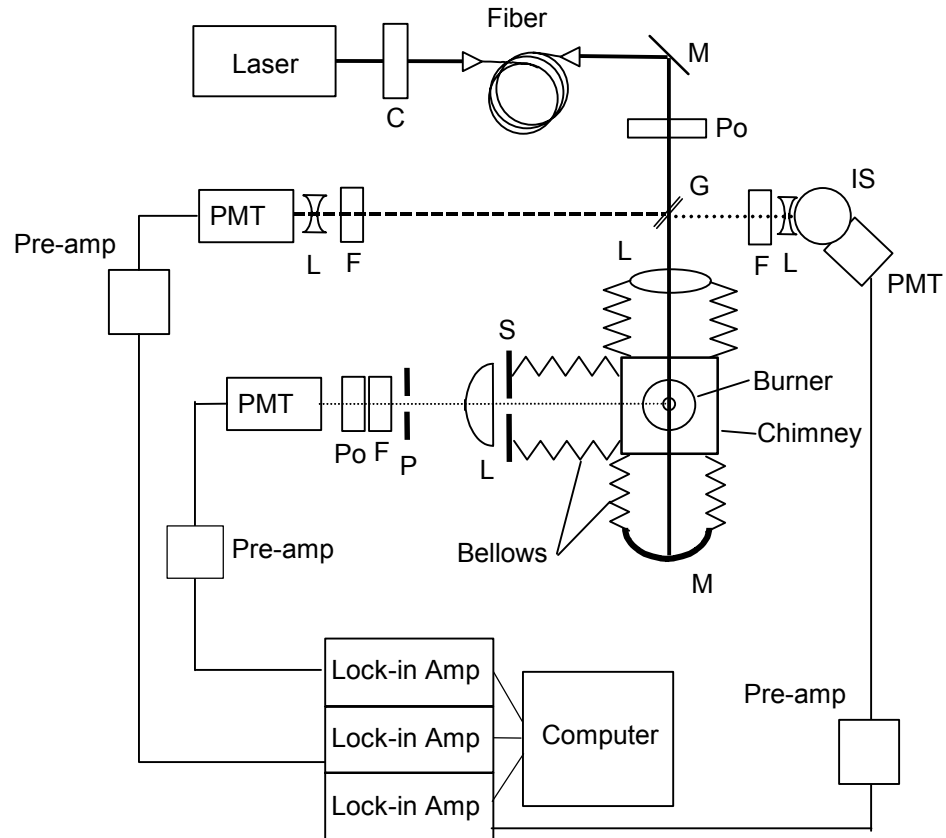


Figure 1: Schematic of laser scattering/extinction system: C, chopper; M, mirror; G, beam pick-off; L, lens; S, spatial filter (circular aperture); Po, polarizer; F, laser-line and neutral density filters; PMT, photomultiplier; P, pinhole; IS, integrating sphere. (Note: Some structural components are not shown, and the drawing is not to scale.)

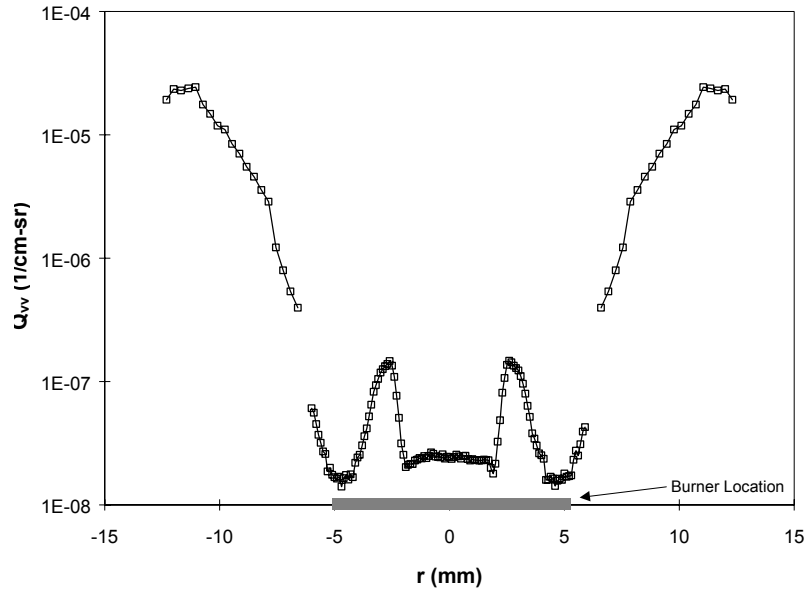


Figure 2: Scattering cross section  $Q_{vv}$  as a function of the radial distance  $r$  from the burner centerline at 7 mm height in stoichiometric  $\text{CH}_4$ -air flame with 200 ppm of  $\text{Fe}(\text{CO})_5$ .

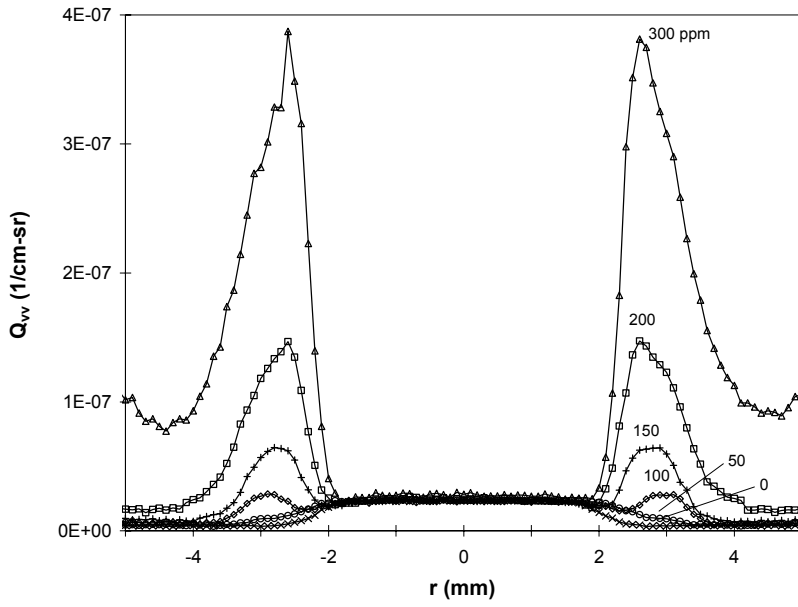


Figure 3: Measured scattering cross section through a stoichiometric CH<sub>4</sub>-air flame 7 mm above the burner rim at various inhibitor mole fractions.

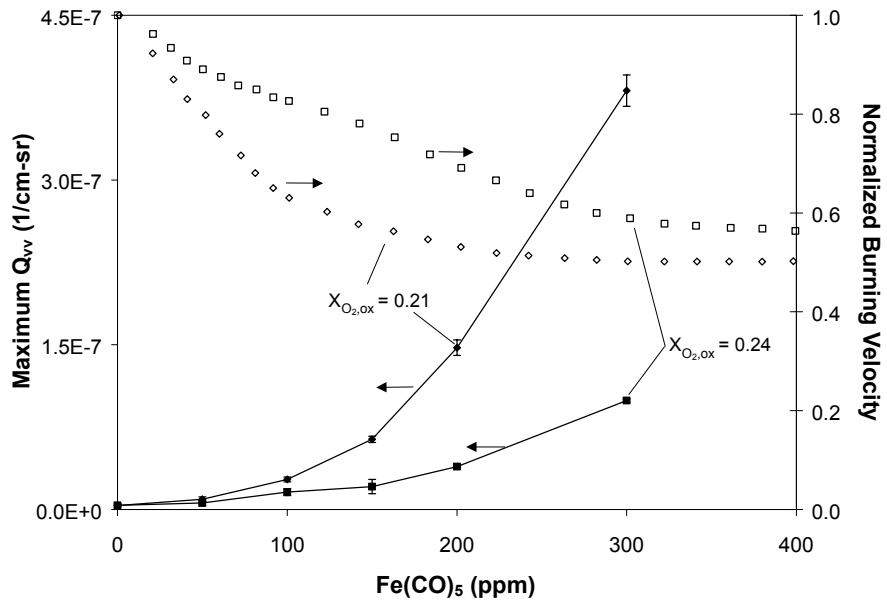


Figure 4: Normalized burning velocity (from Ref. [6]) and maximum  $Q_{vv}$  for  $\phi=1.0$  CH<sub>4</sub> flame with  $X_{O_2,ox} = 0.21$  and  $0.24$ .

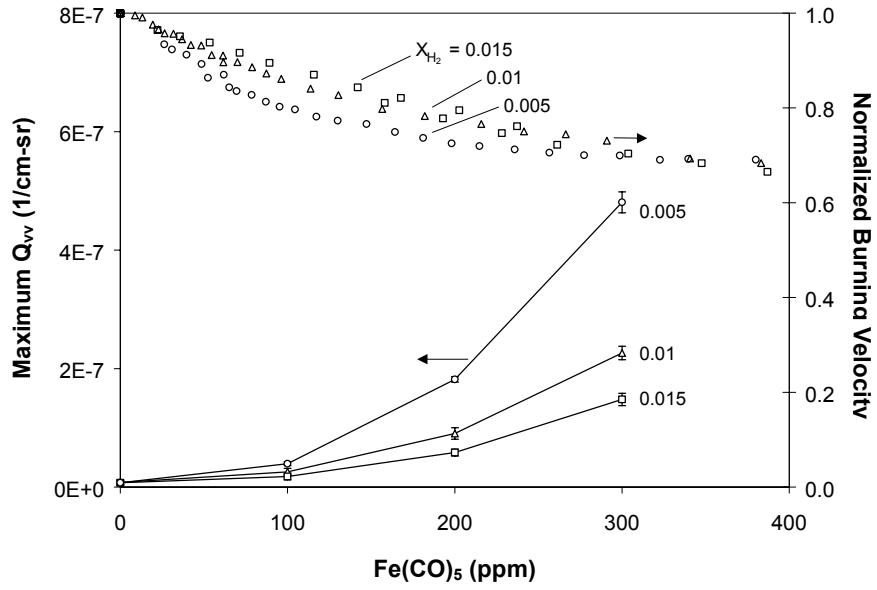


Figure 5: Maximum scattering signal and normalized burning velocity (from Ref.[8]) for CO-H<sub>2</sub> flames as Fe(CO)<sub>5</sub> concentration varies.

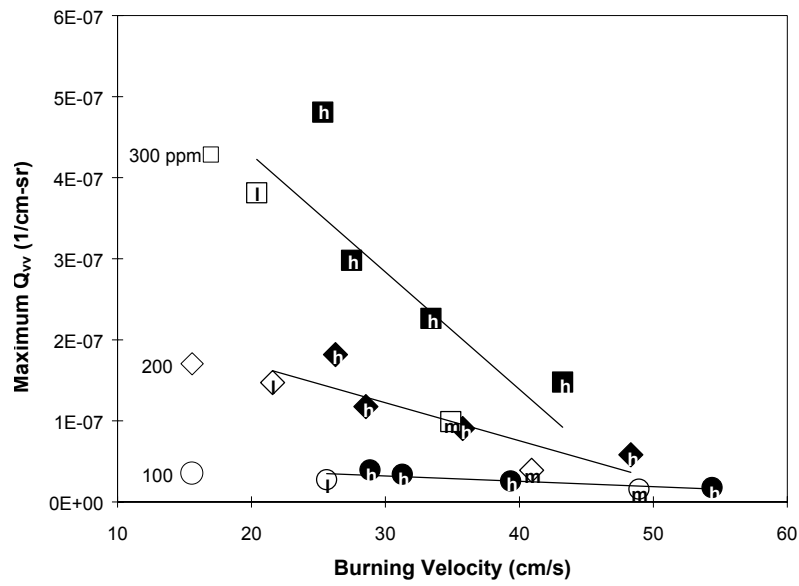


Figure 6: Maximum  $Q_{vv}$  for flames of CH<sub>4</sub> (open symbols) and CO (closed symbols) as a function of the burning velocity (from Ref. [6] and [8]). The letters correspond to the adiabatic flame temperature (l,m,h: low, medium, and high, 2220, 2350, and 2470 K), while the symbol shape (square, diamond, and circle) corresponds to the loading of Fe(CO)<sub>5</sub>: 100 ppm , 200 ppm , and 300 ppm .

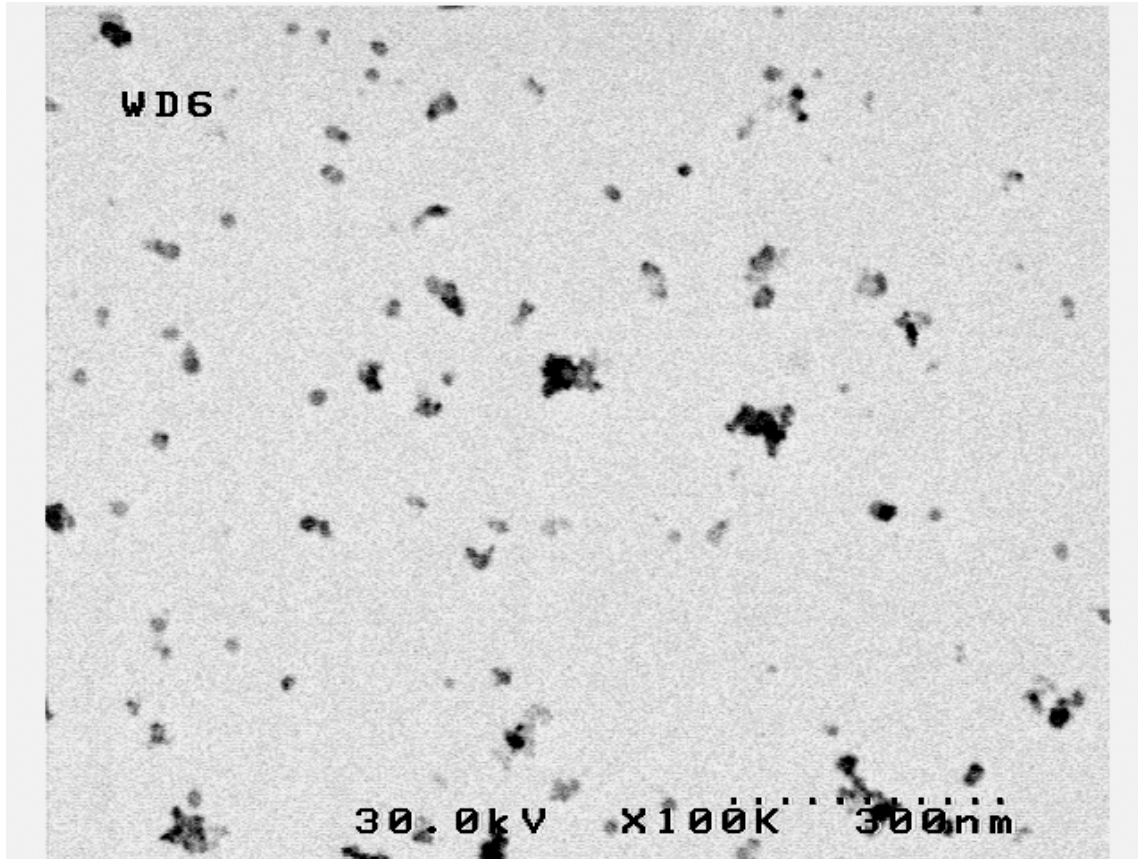


Figure 7: Electron microscope picture of particles sampled from a  $\text{CH}_4/\text{air}$  premixed flame with  $X_{\text{in}} = 200$  ppm.

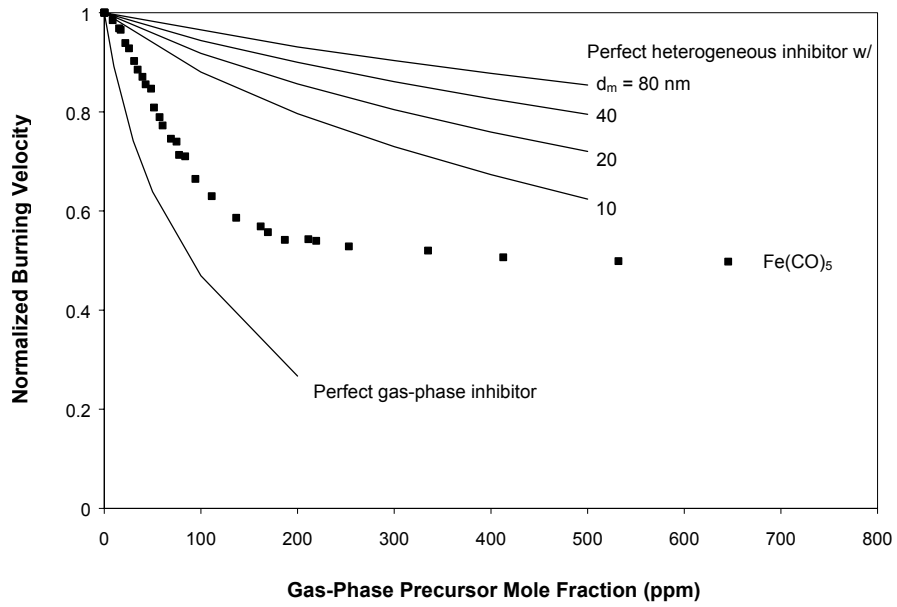


Figure 8: Calculated normalized burning velocity for several diameters  $d_m$  of ideal heterogeneous inhibitor. Also shown are  $\text{Fe}(\text{CO})_5$  data [6], and calculated normalized burning velocity using the perfect gas-phase inhibitor mechanism [7].